INTERNATIONAL JOURNAL OF HYDROGEN ENERGY 47 (2022) 15397–15409

Available online at www.sciencedirect.com

ScienceDirect

journal homepage: www.elsevier.com/locate/he

Graphene functionalization with metallic Pt nanoparticles: A path to cost-efficient H_2 production in microbial electrolysis cells

Pilar Sánchez-Peña [a], Jordi Rodriguez [b], David Gabriel [a], Juan Antonio Baeza [a], Albert Guisasola [a,*], Mireia Baeza [b]

[a] GENOCOV, Departament d'Enginyeria Química, Biologica i Ambiental, Escola d'Enginyeria, Universitat Autònoma de Barcelona, 08193 Bellaterra, Spain

[b] GENOCOV, Department de Química, Facultat de Ciencies, Edifici C-Nord, Universitat Autònoma de Barcelona, 08193 Bellaterra, Spain

HIGHLIGHTS

- Reduced graphene oxide (Pt@rGO) and novel graphitene (Pt@Graphitene) were functionalized with Pt.
- Pt-functionalized graphene-based materials tested as cathodes for MECs.
- Higher surface (24.40 m^2/g) and electroactive (1.14 cm^2) area for Pt@rGO.
- Both materials showed 47% more platinum functionalization than commercial inks.
- Functionalized coating MECs had higher performance than those using commercial inks.

GRAPHICAL ABSTRACT

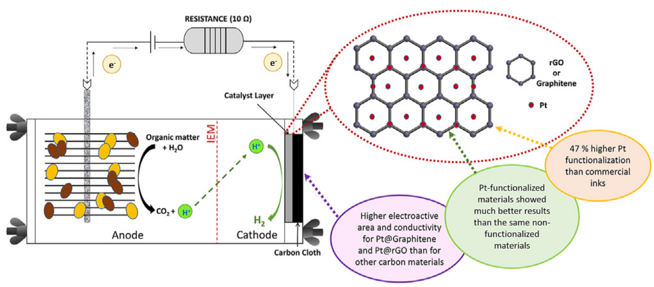

ARTICLE INFO

Article history:
Received 10 November 2021
Received in revised form 4 February 2022
Accepted 9 March 2022
Available online 7 April 2022

Keywords:
Graphitene
Microbial electrolysis cell

ABSTRACT

Platinum is one of the most widely used catalysts in the cathode of Microbial Electrolysis Cells (MECs) to overcome the relatively slow kinetics of hydrogen evolution, even though it is not economically feasible on a large scale. This work aims at developing, applying, characterizing, and optimizing two novel Pt-functionalized inks with promising characteristics: Pt@rGO based on reduced graphene oxide and Pt@Graphitene based on a home-made material named Graphitene, which showed improved performance at a lower cost. The Pt-functionalized materials were deposited on carbon cloth and used as cathode electrode in a single chamber MEC. These materials provided 47% increase in Pt functionalization over commercial inks. Moreover, surface areas of 10.76 m^2/g and 24.40 m^2/g and electroactive areas of 0.10 cm^2/cm^2 and 0.16 cm^2/cm^2 were determined for

* Corresponding author.
E-mail address: albert.guisasola@uab.cat (A. Guisasola).
https://doi.org/10.1016/j.ijhydene.2022.03.078

Novel materials
Pt-functionalization
Reduced graphene oxide

Pt@Graphitene and Pt@rGO, respectively, a difference caused by structural defects in the case of the Pt@rGO, which slightly improved its performance compared to Pt@Graphitene. Thus, the experimental results reached ca. 0.8 mA/cm^2, a 43% higher intensity than that obtained using conventional commercial inks.

Introduction

Hydrogen (H_2) is one promising energy vector to overcome the current dependence on fossil fuels, since it is a clean energy carrier with a high heat of combustion (122 kJ/g) when compared to other possible fuels (coal 40 kJ/g, ethanol 26.5 kJ/g, methane 50.1 kJ/g or petroleum 44 kJ/g [1]). Furthermore, H_2 has a large number of industrial applications as it is employed for hydrogenation in the production of petrol, food and fertilizers. However, almost 90% of the H_2 produced comes from steam reforming [2], a fossil-based, non-sustainable technology that hinders future H_2 utilization. Thus, research is focused nowadays on developing novel CO_2-free technologies for H_2 production. Among them, biological approaches stand as some of the most sustainable. Currently, there are three alternatives for biological H_2 production [3]: photosynthesis, dark fermentation, and microbial electrolysis cells (MECs).

MECs are bioelectrochemical devices that raise a promising new approach to H_2 production from the organic compounds contained in wastewater [4], thus with a double contribution to a sustainable economy. A MEC operates as a potentiostatic cell consisting of an anode and a cathode connected to a power source, *i.e.* with a constant cell potential. The anode is colonized with anode-respiring bacteria (ARB), which act as a catalyst to oxidize organic matter into electrons, CO_2 and H^+. ARB have the unique characteristic of being able to transfer electrons extracellularly to the anode, which subsequently are circulated to the cathode [4]. Several reductive processes are reported to occur at the cathode [5–7]. However, in MEC, the conventional process is the reduction of H^+ or H_2O to H_2 gas. MECs can be operated in single or two-chamber mode. In a two-chamber MEC, the anodic and cathodic chambers are usually separated by an ion-exchange membrane (IEM) whereas the anode and cathode coexist in a sole chamber in single-chamber MECs. The lack of membrane reduces transport resistance at expenses of promoting the growth of hydrogen scavengers [8] such as hydrogenotrophic methanogens [9], hydrogen oxidizing ARB [10] and homoacetogens [11], which can limit considerably the observed H_2 production yield [12].

MECs have provided very promising results under lab-conditions with H_2 production raets up to 1–3 m^3 H_2/m^3 reactor/d [13–15]. However, a successful scale-up has not been reported yet [16,17]. One of the hurdles to overcome is the actual need of an expensive catalyst in the cathode to drive H_2 evolution. The most common catalyst used is platinum (Pt) and, thus, there is a need of finding cheaper alternatives to ensure the economic viability of full-scale MECs [9,18]. Pt-coated carbon-based materials are the most common materials for cathodes, but there are also promising alternatives such as those based on nickel [19], titanium [20] or stainless steel [21], which have demonstrated good performance. These metals have similar chemical and physical properties to Pt and can provide high catalytic activity for H_2 production [20]. However, a replacement of Pt that provides a similar performance at a lower price has not been reported yet. In this context, an alternative option is to minimize the amount of Pt added to the cathode without hindering its activity. For instance, decreasing the Pt particle size into the nanoscale (2–3 nm) and functionalizing the cathode with Pt nanoparticles would lead to great benefits due to the increase of the Pt surface area while minimizing the amount of Pt required on the cathode surface and increasing Pt availability [22]. This functionalization has been reported to be successful on carbon based materials such as graphene or carbon nanotubes [23,24], even though to the best of our knowledge they have not been used for MECs.

On the other hand, graphene is a carbon-based novel material that has been widely studied since the report of its physical properties back in 2004 and 2005 [25,26]. Graphene is a single layer of sp^2-hybridized carbon atoms arranged in a honeycomb crystal structure. Its large surface area and the 2-D carbon network of flat basal planes makes graphene effortlessly modifiable [27]. Besides that, its synthesis and functionalization are cheaper than buying a commercial ink. The best known modification of graphene is reduced Graphene Oxide (rGO) [28]. rGO is a single-atom-thick, two-dimensional material with carbon ring domains, defects, and oxygen-containing groups (-OH, –COOH, etc.) on the surface [29]. Furthermore, rGO has a higher conductivity compared to other carbonaceous materials, thus becoming a perfect candidate for cathodic material of MECs in combination with Pt. In fact, graphene-based electrodes have already been used in a different type of bioelectrochemical systems: microbial fuel cells [30–32]. For this purpose, rGO could be functionalized with Pt metal nanoparticles. According to Georgakilas et al. [33], two approaches for an organic covalent Pt functionalization reaction are basically available: (i) the formation of covalent bonds between a free radical and a C=C bond of pure graphene; (ii) the formation of covalent bonds between an organic functional group and an oxygenated aliphatic domain [34].

This work aims at reporting the novel utilization of graphene functionalized with Pt nanoparticles as cathode for efficient bioelectrochemical H_2 production. Two different types of graphene were synthesized: i) rGO derived from graphene oxide prepared according to the traditional Hummers' method [35,36] and reduced with 2 mM ascorbic acid and ii) a low-cost material, namely graphitene, composed of graphene particles with a broader distribution in the number of layers, which was home-made with a simple and highly scalable ball-milling procedure.

Materials and methods

MEC design

The MEC configuration used in this work was a 28 mL methacrylate cylindrical vessel with a glass cylinder on top (16 mL), and a total working volume of 35 mL (Fig. 1). The glass cylinder was hermetically closed with a PTFE rubber cover and aluminium crimp, which allowed gas to be collected [37]. The anode was a graphite fibre brush (20 mm diameter x 30 mm length; 0.21 m^2) made with type PANEX33 160 K fibres (ZOLTEK) of 7.2 μm of diameter, thermally treated and connected with a titanium wire core. The cathode was prepared with the different Pt-functionalized graphene materials.

The gas produced was recovered with a gas-tight bag (Ritter, Cali-5-bond) connected with a PVC tube to the glass cylinder. The cathode and the anode were connected to a power supply (Velleman Energy, LABPS3005DN) that applied a constant potential of 0.80 V. Current production was calculated by measuring the voltage drop across a 10 Ω external resistance that was connected in series to the circuit and applying Ohm's law. The cells worked in batch mode with sodium acetate (initial concentration in the batch: 1.5 g/L) as electron donor.

Functionalization of rGO with Pt

rGO was produced following the Hummers' method [38] and, afterwards, it was functionalized with K_2PtCl_4. For the rGO production, 1 g of graphite flakes (particle size +100 mesh, Sigma-Aldrich, Spain), 23 mL of H_2SO_4 and 0.5 g of $NaNO_3$ were added in a stirred 500 mL Erlenmeyer, and later cooled down in an ice bath as the reaction is exothermic and needs to be cooled. Then, 3 g of $KMnO_4$ were slowly dosed in the reaction medium and, afterwards, all the solution was heated up to 45 °C for 30 min to promote oxidation. When the material was oxidized, the colour changed from black to dark brown and the solution was allowed to cool down to room temperature. Deionized water (46 mL) was added to reduce the acidity of the medium and the mixture was shaken magnetically for 15 min. The solution was later treated with 140 mL of deionized water for Milli-Q system (Millipore, Billerica, MA, USA) and 2.5 mL of H_2O_2 to remove the excess of MnO_4^- and MnO_2 as $MnSO_4$. The solution was washed with 10% of HCl solution and centrifuged at 3500 rpm as many times as necessary to remove a yellow viscous liquid (undesired reaction by-products). The solid product, graphene oxide, was washed with deionized water and centrifuged to reach a neutral pH and was dried at 80 °C for 24 h.

Then, the resulting solid was mixed with deionized water and was sonicated for 1 h to separate the different sheets of graphene oxide. The pH was increased up to 9~10 with an ammonium chloride solution (25% wt) to stabilize the graphene oxide sheets. Then, ascorbic acid (2 mM) was added and the solution was heated up to 95 °C. Finally, the final product, rGO, was centrifuged at 3500 rpm and washed with deionized water until neutral pH was obtained. The resulting solid was dried at 80 °C for 24 h.

Pt was functionalized with a novel methodology based on the addition of Pt to the carbon materials through a covalent bond between Pt and the free radical or C=C bond [39]. 140 mg rGO were mixed with 100 mL of deionized water and were sonicated for 1 h. 104.1 mg of K_2PtCl_4 were added to the mixture and mixed for 30 min. Meanwhile, a solution of 0.1 M of $NaBH_4$ was added drop by drop. Then, the solution was mixed for 1 h. The mixture was taken to neutral pH by washing with deionized water and centrifugation. Then, the product dried overnight at 100 °C is referred as Pt@rGO herein.

Ascorbic acid (99.5%), DMF (99%), hydrochloric acid (30–35%), hydrogen peroxide (30%), nitric acid (65%), potassium permanganate (99.99%), potassium tetrachloroplatinate (II) (>99.99%), sodium nitrate (99.0%), sodium borohydride (98%), sulphuric acid (95–98%) and Nafion perfluorinated

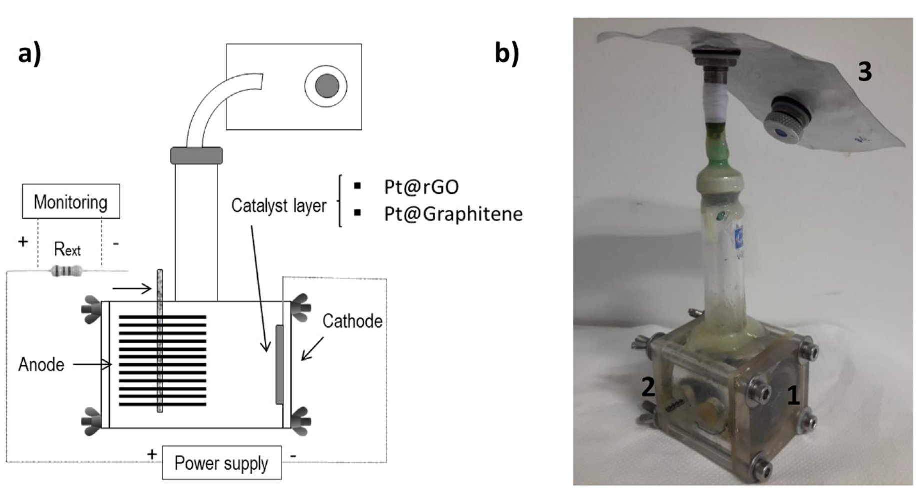

Fig. 1 – Schematic (a) and picture (b) of the MEC (1: anode, 2: cathode, 3: H_2 collection).

resin solution were purchased from Sigma-Aldrich (St. Louis, MO, USA).

The catalyst ink was obtained by mixing the rGO functionalized with Pt (0.5 mg Pt/cm^2), and Milli-Q water (4.25 μL/cm^2) during 20 s. Later, Nafion (33.4 μL/cm^2) (Figs. S1 and S2) and, N-dimethylformamide (16.7 μL/cm^2) were added to obtain a bonding paste and the solution was stirred again (Fig. S3). The resulting paste was coated over the carbon cloth using a thick brush. The final layer was air-dried for a period of 24 h (Fig. S4). Finally, a titanium wire was assembled to the carbon cloth so the cathode could be electrically connected. The same procedure was carried out with non-functionalized rGO for comparison purposes.

Functionalization of graphitene with Pt

Graphitene is the name we have given to a carbon material with between 4 and 20 layers of graphene, being the material a mix of graphene and graphite. Graphitene was obtained from GraphCat Community (Graphene community of Catalonia). This material combines the benefits of graphene (large active surface and high conductivity due to the lack of defects) with a low cost and easy scalability.

The first step in the Graphitene functionalization was the activation of its surface with carboxylic groups by dispersing Graphitene in a 2.5 M nitric acid and placing the solution in an ultrasound bath for 2 h. Deionized water followed by centrifugation was used to wash the mixture to reach pH 7.0. 140 mg of Graphitene were mixed with 100 mL of deionized water and sonicated for 1 h. 104.1 mg of K_2PtCl_4 were added to the mixture and stirred for 30 min. Afterwards, 100 mL of 0.1 M of $NaBH_4$ were added drop by drop. Then, the mixture was stirred for 1 h. Finally, it was rinsed with deionized water followed by centrifugation until reaching pH 7. The product dried overnight in an oven at 100 °C is referred as Pt@Graphitene herein.

Nitric acid (65%), sodium borohydride (98%), potassium tetrachloroplatinate (II) (>99.99%), DMF (99%) and Nafion perfluorinated resin solution were purchased from Sigma-Aldrich (St. Louis, MO, USA).

The catalyst ink was obtained by mixing the Pt@Graphitene (0.5 mg Pt/cm^2) and Milli-Q water (4.25 μL/cm^2) during 20 s. Then, Nafion (33.4 μL/cm^2) and N,N-dimethylformamide (16.7 μL/cm^2) were added and stirred to produce the binder paste, which was coated over the carbon cloth using a thick brush. The resultant layer was air-dried for 24 h (Fig. S4). Finally, a titanium wire was assembled to the carbon cloth so the cathode could be electrically connected. The same procedure was carried out with non-functionalized Graphitene for comparison purposes.

Analytical methods and instrumentation

Samples for chemical analysis were taken at the beginning and at the end of each cycle, representing a maximum of 10% of the complete reactor volume. Acetate in selected samples was analysed with a gas chromatograph (Agilent Technologies, 7820-A), employing a DB-FFAB column (30 m of length, 250 μm of internal diameter and 0.25 μm of film thickness), a flame ionization detector and He as carrier gas [40].

Some materials were studied and morphologically characterized using Scanning Electron Microscopy (SEM) and Transmission Electron Microscopy (TEM). SEM measurements were carried out in a Merlin Zeiss microscope operated at 5 kV and with an EDX detector (SEM-EDX) analysis system and Jeol JSM 6010 (JEOL, Ltd, Tokyo, Japan) [41]. TEM images were obtained with the JEOL 1400 microscope operated a 120 kV. The Gatan Microscopy Suite Software was used for the analysis of electron diffraction. When necessary, particularly for the external cathode side, a thin carbon film was used to coat the samples, by thermal evaporation of carbon, to avoid any misleading charging effect [42].

The percentage of Pt was analysed using plasma mass spectroscopy (ICP-OES) by an inductively coupled plasma optical emission spectrometer (Perkin, Elmer, model Optima 4300DC) with a Milestone microwave digester (model Ultrawave). Between 1.5 and 2 mg of each sample were weighed on a microbalance (MX5, Mettler Toledo) and digested, in duplicate, with water in a microwave oven. Finally, the amount of Pt was determined by ICP-OES spectrometry.

The Brunauer, Emmett and Teller (BET) technique was used to estimate the surface area of the cathodes. A Micromeritics ASAP 2000 unit was used, using N_2 as adsorption/desorption gas.

The oxidation state of Pt was analysed with photoemission spectroscopy (XPS) at room temperature in a SPECS PHOIBOS 150 hemispherical analyser (SPECS GmbH, Berlin, Germany). The base pressure was $5 \cdot 10^{-10}$ mbar using monochromatic Al K-alpha radiation (1486.74 eV) as excitation source operated at 300 W. The energy resolution as measured by the Full-Width Half-Maximum of the Ag 3d5/2 peak for a sputtered silver foil was 0.62 eV.

Both electrodes were connected to a power supply (Velleman LABPS3005DN) with 0.8 V as applied potential. The voltage across external resistances was measured with a data acquisition card with 16-bit resolution (Advantech PCI-1716) installed in a computer where the AddControl programm, a propietary software developed in LabWindows/CVI2019 by the research group, was used for data management and storage.

H_2, CH_4, and CO_2 were measured with a gas chromatograph (Agilent Technologies, 7820-A) equipped with two columns, a packed column Porapaq Q 80/100 3 ft G3591-81136 (1.38 m × 2 mm) and a second column MolSieve 5 A 80/100 3 ft. G3591-80017 (1.83 m × 2 mm), from Agilent Technologies. N_2 was used as carrier gas. The temperature of the oven was initially set at 70 °C for 2 min, followed by a ramp of 20 °C· min^{-1} until reaching a temperature of 140 °C. Dionex Chromeleon 6.8 (ThermoFisher Scientific) was used for data acquisition and processing to estimate the concentrations of each gas.

Electrochemical techniques

The MEC performance was assessed using electrochemical techniques, in which an abiotic anode was used to assess the global cell and cathode performance without being biased by the activity of a biofilm on the anode. These techniques were applied in a three-electrode configuration and single methacrylate cell in all cases, employing the same abiotic anode for all the cathodes. A commercial Ag/AgCl electrode (BioLogic) with KCl 3 M internal solution was used as reference electrode.

Electrochemical impedance spectroscopy

Electrochemical impedance spectroscopy (EIS) measurements are helpful to gather performance information of electrodes (anode or cathode) [43,44]. EIS experiments were performed using a potentiostat/galvanostat with a frequency analyser (Autolab PGSTAT302 N, Methrom Inc.). A three-electrodes configuration was used to analyse the cathode performance: the cathode as the working electrode, the anode as the counter electrode, and an Ag/AgCl electrode as the reference electrode. EIS analyses were recorded in the frequency range 100 kHz - 10 mHz at open-circuit potential. The amplitude was set to 1 mV at AC to avoid detachment of the biofilm and to reduce perturbations of steady state conditions of the cell [41]. In addition, acetate was added to prevent it from being the limiting factor and nitrogen was purged for 30 min to simulate real conditions in the cell.

The circuit used for fitting the results was a simplified version of the Randles circuit without the Warburg element [45]. Fig. 2 shows the circuit and corresponding Nyquist plot, where R_s is the ohmic resistance (related to the resistance of the electrolyte and components, such as electrodes or membranes), R_{ct} is the charge resistance (related to the difficulty of the electrons to flow) and C_{dl} is the capacitance (related to the double electrolytic layer).

Cyclic voltammetry

The amount of electroactive surface area was tested by cyclic voltammetry (CV), employing a potentiostat/galvanostat (Autolab PGSTAT302 N, Methrom Inc.). CV measurements were executed using the three-electrode configuration as in section: Electrochemical impedance spectroscopy. The redox pair $Fe(CN)_6^{4-}/Fe(CN)_6^{3-}$ was the redox marker in a 100 mL of 0.1 M KCl solution containing 0.01 M $K_4Fe(CN)_6/K_3Fe(CN)_6$ under quiescent condition. The oxidation of $Fe(CN)_6^{4-}$ and the reduction of $Fe(CN)_6^{3-}$ on the surface of the working electrode created anodic and cathodic currents, respectively:

$$[Fe(CN)_6]^{-4} \leftrightarrow [Fe(CN)_6]^{-3} + 1\ e^- \quad (1)$$

The intensity (I_p) was proportional to the electroactive surface area of the cathode (equation (2), Randles-Ševčik equation [46]).

$$I_p = 268600 \cdot n^{3/2} \cdot A \cdot D^{1/2} \cdot C \cdot v^{1/2} \quad (2)$$

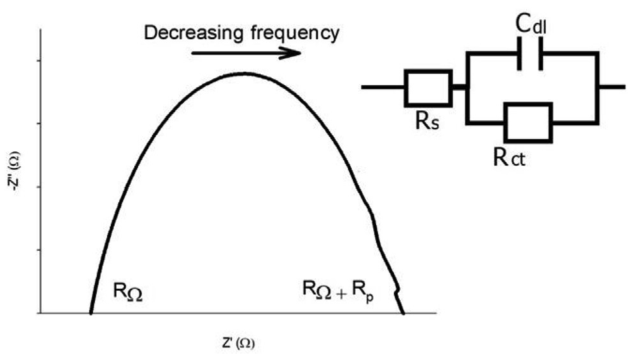

Fig. 2 – Nyquist plot of EIS with the corresponding elements.

being I_p (A) the peak intensity, n the electrons transferred in the reaction, A (cm^2) the electroactive surface area, D ($6.4 \cdot 10^{-6}$ cm^2/s) the $Fe(CN)_6^{4-}$ diffusion coefficient in water, C (mol/cm^3) the concentration of the reaction species in the solution and v (V/s) the scan rate (0.005 V/s).

Calculations

The intensity was calculated with the voltage measured across the external resistance and the Ohm law (equation (3)):

$$I = E/R_{ext} \quad (3)$$

being I the current (A), E the voltage (V) and R_{ext} the external resistance (Ω).

The Coulombic Efficiency (CE), equation (4), is a common indicator of the MEC performance and it corresponds to the ratio of electrons recovered as current vs those contained in the organic matter degraded in the anode.

$$CE = \frac{\int_{t_0}^{t_F} I\, dt}{F \cdot b_S \cdot V_L \cdot \Delta c \cdot M_S^{-1}} \quad (4)$$

being t_0 and t_F (s) initial and final time of the batch, I (A) the current, F (96,485C $mol^{-1} \cdot e^{-1}$) the Faraday's constant, b_S the e^- transferred per mole of substrate, V_L (L) the volume of liquid in the reactor, ΔC ($g \cdot L^{-1}$) the concentration of substrate consumed in a batch and M_S ($g \cdot mol^{-1}$) the substrate molecular weight.

The performance of the MEC was also evaluated using the cathode gas recovery (r_{CAT}), equation (5), which corresponds to the ratio of electrons recovered as H_2 to the electrons flowing from the anode to the cathode as current:

$$r_{CAT} = \frac{b_{H_2} \cdot V_{H_2} \cdot F \cdot V_m^{-1}}{\int_{t_0}^{t_F} I\, dt} \quad (5)$$

being b_{H2} the moles of e^- transferred per mole of H_2 (2 mol $e^- \cdot mol^{-1} \cdot H_2$), V_{H2} the volume of hydrogen produced, and V_m the molar gas volume (24.03 L mol^{-1}) at 20 °C.

The H_2 relative composition was evaluated using equation (6):

$$\text{Relative composition}_{H_2} = \frac{V_{H_2}}{V_{H_2} + V_{CH_4}} \quad (6)$$

where V_{H2} and V_{CH4} represent the volume of H_2 and CH_4 produced, respectively.

The amount of gas was estimated according to the “Gas Bag Method” presented by Ambler and Logan [47]. The method starts with a first analysis of the gas composition in the gas collection bag. Then, a known volume of a reference gas, in this case, carbon dioxide, is added to the gas collection bag and the composition of the resulting mixture is analysed again. From these two analyses and proper mass balances, the total initial volume in the bag ($V_{total,\ initial}$) can be calculated using equation (7).

$$V_{total,\ initial} = \frac{V_{added,\ CO_2}(1 - x_{run\ 2,\ CO_2}) + V_{run\ 1}(x_{run\ 2,\ CO_2} - x_{run\ 1,\ CO_2})}{x_{run\ 2,\ CO_2} - x_{run\ 1,\ CO_2}} \quad (7)$$

where $V_{added,CO2}$ is the known volume of carbon dioxide added, $V_{run\ 1}$ is the volume obtained for the first GC analysis, and $x_{run\ i,\ CO2}$ is the molar fraction of carbon dioxide in the analysis number i.

Results and discussion

Assessment of Pt functionalization

In a first step, both carbonaceous materials, i.e. Graphitene and rGO, were functionalized with Pt. The functionalization yield, i.e. the total amount of Pt adhered over each material, was quantified by quintuplicate through ICP-OES. The percentage of Pt functionalization (i.e. the amount of Pt in the nanomaterial) was 18.4 ± 2.4% for Pt@rGO and 19.7 ± 5.0% for Pt@Graphitene. Thus, Pt@Graphitene had a slightly higher average content but also a higher standard deviation. The success of this Pt-based functionalization is already a relevant outcome of this work since the obtained Pt@rGO and Pt@Graphitene showed a higher proportion of Pt than other commercial inks used as catalyst in MECs (≈10% Pt content) [48]. In addition, the functionalization percentages are up to three-fold higher than those reported for the functionalization of similar materials (Table 1).

The morphological characteristics of the internal side of the cathode, i.e. the side in contact with the solution, were studied using SEM. Fig. 3 shows the SEM images of the Pt distribution of both synthesized powder materials before they were deposited in the carbon cloth. Pt@rGO are tiny crystals with white dots (corresponding to Pt). Contrarily, Pt@Graphitene presents larger crystals also displaying the Pt-related white dots. Pt@rGO crystals are more fragmented than Pt@Graphitene crystals and, therefore, they would be *a priori* easier to disperse.

Both carbonaceous materials functionalized with Pt, i.e. Pt@Graphitene and Pt@rGO, were used to prepare two different cathodes. Fig. 4 shows the SEM images of the functionalized materials when deposited on the carbon cloth surface. The Pt and C distribution was evaluated through SEM-EDX through a mapping of the surface (Figs. S5 and S6). Pt was homogeneously distributed in both cases and, thus, it can effectively be used for H_2 evolution reaction as a catalyst. Besides that, the Pt@rGO (Fig. S5) showed finer crystals, which is a preferred scenario since the electrode coating is more efficient. The ink with finer crystals should be less prone to come off when entering in contact with the mineral medium and, thus, should be more stable. Moreover, the Pt@Graphitene (Fig. S6) covered less cathodic area because of the larger crystals. Also, Pt detachment was qualitatively observed with the naked eye since the medium became darker. Finally, larger crystals resulted in a more scattered global Pt distribution on the cathodic surface. According to the SEM observations, Pt@rGO would be preferred as it is easier to disperse and less prone to detachment.

Furthermore, the electron diffraction and the crystallinity of the different materials were studied through TEM (Fig. 5). The Pt@rGO electron diffraction showed a well-ordered material with a perfect hexagonal structure (Fig. 5a), which indicated the presence of only a few layers of material. On the other hand, Pt@Graphitene showed a crystal structure (Fig. 5b) but the hexagon was not visible. Pt@Graphitene showed many messy layers and the TEM electron beam could not be focused properly, showing a more amorphous material. Pt@Graphitene showed a circular figure composed of many hexagons in different positions, each one corresponding to a crystalline plate and, therefore, to a sheet of material. Thus, the higher the number of material layers, the less superficial area, and thus, the lower current density. Furthermore, the distance between planes was extremely similar (around 1.11 nm in both cases), even though Pt@rGO had more defects than Pt@Graphitene.

The size of the Pt nanoparticles was also studied by TEM. The nanoparticles size varied between 8 and 38 nm for Pt@rGO (Fig. S7) and 12 and 87 nm for Pt@Graphitene (Fig. S8) with an average size of 23 ± 5 nm and 35 ± 12 nm for Pt@rGO (n = 100) and Pt@Graphitene (n = 100), respectively. This average size was higher than that obtained in previously reported graphene functionalization [22] but lower than the Pt size in a commercial ink [57]. The lower the size of the nanoparticles, the higher the superficial area and, thus, the higher availability of Pt (where the electrochemical reaction takes place). A BET analysis was conducted to evaluate the surface area and pore size distribution of the different inks before and after their Pt functionalization. The surface area results were 12.39 m^2/g and 24.40 m^2/g for rGO and Pt@rGO, respectively,

Table 1 – Comparison of the yield of different functionalization in carbon materials based on graphene.

Carbon material	Functionalized with	% (wt) of functionalization	Ref.
Pt@Graphitene	Pt	19.7 ± 5.0	This work
Pt@rGO	Pt	18.4 ± 2.4	This work
Graphene	Pt	16.61	[23]
rGO	Pt	7.41	[49]
GO	Pt	3.61	[39]
Graphene	Fe@Au	13	[50]
Graphene	Nitrogen	9.5	[51]
Graphene	Nitrogen	5.74	[52]
Graphene	Nitrogen	<2 (9% atomic percentage)	[53]
Graphene	Nitrogen	8.9	[54]
Graphene	Porphyrin	5	[55]
Graphene	Poly (acrylonitrile)	1	[56]
	Poly (methylmethacrylate)	0.05	

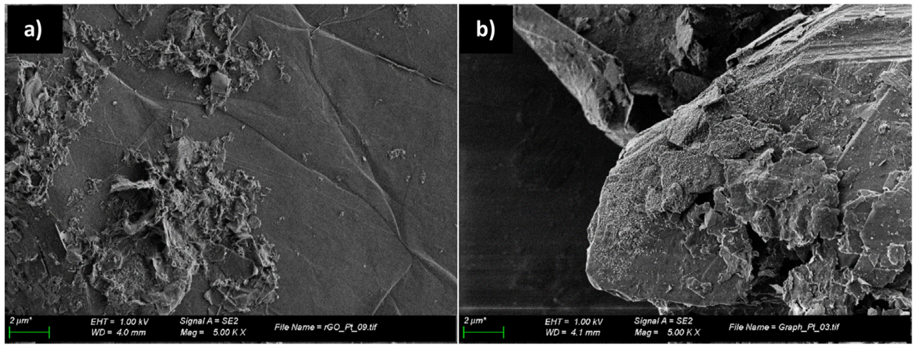

Fig. 3 – SEM images of both graphenes functionalized: Pt@rGO (a) and Pt@Graphitene (b).

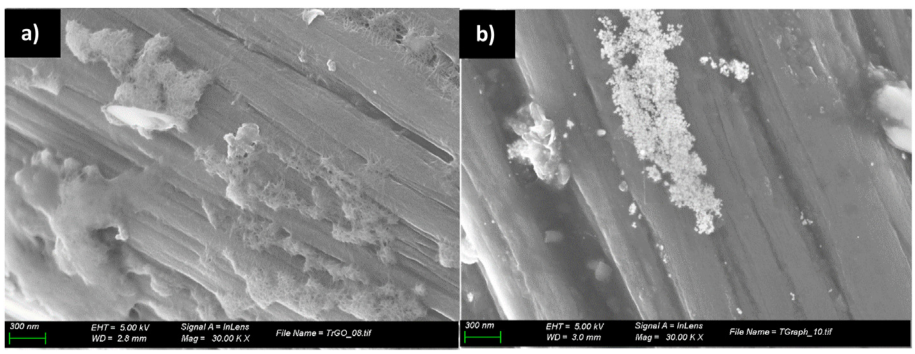

Fig. 4 – SEM images of the cathodes with ink based on Pt@rGO (a) and Pt@Graphitene (b).

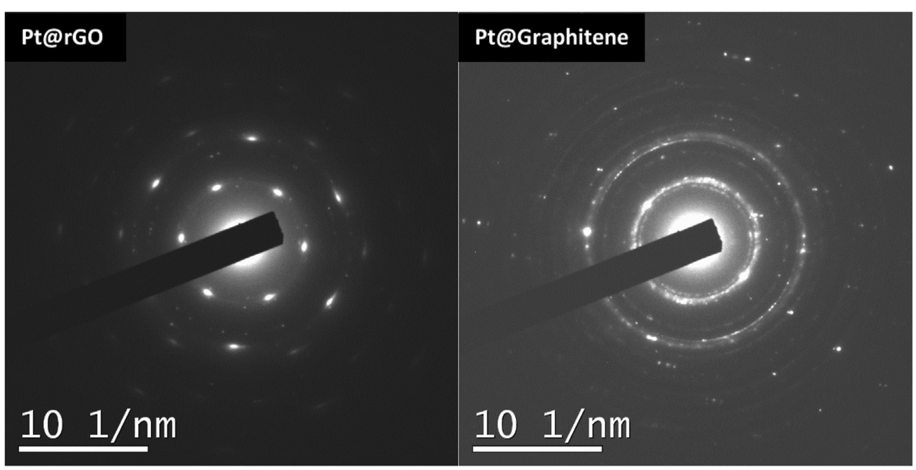

Fig. 5 – Electron diffraction of Pt@rGO and Pt@Graphitene.

and 5.80 m^2/g and 10.76 m^2/g for Graphitene and Pt@Graphitene, respectively. The superficial area increased when the materials were functionalized because Pt induced a separation of the layers, thereby raising the active area. In addition, rGO had a higher initial surface area than Graphitene since rGO had more defects in its structure, such as carbonyl, hydroxyl, or phenol groups. Moreover, rGO had a lower amount of graphene per gram of Pt@Graphitene while a higher surface area was found for Pt@rGO compared to that of Pt@Graphitene. Comparing Figs. S5 and S6, a large number of defects can be observed in the Pt@rGO structure compared to that of Pt@Graphitene, which was related with a higher oxygen content in Pt@rGO. Besides, Pt nanoparticles were smaller in Pt@rGO leading to a more homogenous distribution and a higher electroactive area.

Finally, the oxidation state of Pt in both materials was analysed using XPS. Both Pt@rGO and Pt@Graphitene presented peaks in 71.00 and 74.95 eV with similar intensities, which corresponds to metallic Pt and PtO_2 [58] (see Fig. S9). The Pt functionalization process was reproducible and both materials had a similar amount of Pt and a similar proportion of metallic Pt and PtO_2. Metallic Pt is the catalyst of the hydrogen evolution reaction and, therefore, 50% of the Pt on the cathode could be used as catalyst. This value is in the high-end of the range of other reported Pt-based cathodic materials. For instance, the commonly-used commercial ink presented peaks in 71.93 and 74.99 eV, indicating that the Pt distribution was approximately, 50% of PtO_2, 25% of PtO and 25% of metallic Pt. Thereby, both Pt@rGO and Pt@Graphitene had around two-fold proportion of metallic Pt than the commercial ink and, thus, higher catalytic activity.

Electrochemical characterization: CV and EIS measurements

CVs were conducted with both materials (Fig. S10) to determine the electroactive area using the intensity of the oxidation peaks (positive intensity values) and equation (2), the current peak. The CVs showed two peaks related to the oxidation and reduction of iron. The electroactive area of Pt@rGO and Pt@Graphitene corresponded to 1.14 and 0.69 cm^2, respectively, confirming the higher availability of Pt in Pt@rGO, which correspond to 0.16 cm^2/cm^2 and 0.1 cm^2/cm^2, respectively, once normalized with respect to the surface area of the electrode. These values are lower compared with the geometric area (7 cm^2) but a 13% higher compared with the commercial ink (0.60 cm^2).

Fig. 6 shows the Nyquist diagrams for the EIS measurements for the three Pt-based cathodes tested in this work. Table 2 shows the characteristic EIS parameters obtained for each experiment. R_s (related to the ohmic resistance) were similar in both functionalized cells because both used the same solvent and electrode, the major contributors. Regarding R_{ct} (related to the charge resistance), Pt@rGO showed less than half the R_{ct} of Pt@Graphitene because the Pt distribution on the cathode was more homogeneous and the ink was less scattered throughout its domain. Consequently, the electronic transfer was favoured. Furthermore, Pt@rGO showed a slightly higher surface area for the electrochemical reaction to take place.

Over a 250% higher resistance was found for the cell with Pt/C commercial because of the higher carbon content of the cathode coated with the Pt/C ink and because of its lower Pt availability, as the amount of ink needed to obtain the same ratio of Pt/cm^2 was around 50% higher. Besides that, the

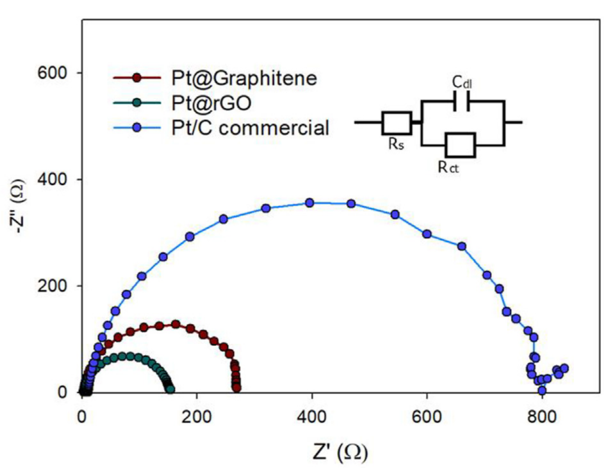

Fig. 6 – EIS of different carbon materials functionalized with Pt, obtained using a frequency range of 100 kHz to 10 mHz. Randles circuit: Rs·(Rct·Cdl) (inset).

Table 2 – Resistances obtained in the simplified Randles equivalent circuit in cells with Pt@rGO, Pt@Graphitene and standard cathodes.

	R_S (Ω)	R_{ct} (Ω)
Pt@rGO	2.9	151.0
Pt@Graphitene	2.8	266.1
Pt/C Commercial	10.5	788.0

transducer capacity of rGO and Graphitene improved compared with other carbon materials leading to a reduction on cell resistance. Resistance for both Pt-functionalized coatings was lower than that reported for other carbon materials, i.e. graphene oxide modified with non-imprinted polymer provided 3974 Ω [59] while a non-functionalized graphene surface showed a R_{ct} of around 6000 Ω [60]. Consequently, such reduction on cell resistance in the materials studied herein caused such increase in performance of the cells.

These novel nanomaterials reported herein facilitated the electrochemical reaction to take place on the electrode surface due to a higher Pt availability and an improved electronic transfer of material. Furthermore, compared with other BES, our cells showed an order of magnitude lower cell resistances than other previously reported [61].

Performance assessment of the cells

Eight MECs were built using cathodes coated with the different carbonaceous materials manufactured in this work (rGO and Graphitene, and Pt@rGO and Pt@Graphitene) and were operated for more than two months under cyclic, repetitive conditions. Fig. 7 shows the current density evolution obtained for these MECs during the last 18 days of operation (i.e. under pseudo steady-state conditions). The cells with cathodes containing Pt@rGO and Pt@Graphitene provided an average current density of 0.78 and 0.71 mA/cm^2, respectively, whereas these values decreased to 0.25 and 0.22 mA/cm^2 for rGO and Graphitene, respectively, due to the lack of Pt functionalization.

Current densities obtained remained relatively stable during the operation of the cells (more than two months). No catalyst detachment or corrosion was detected that could have affected the performance of the material during the period of operation and, therefore, the material was not only structurally stable, as indicated in section: Assessment of Pt functionalization (Appendix A), but also had stable electrical and chemical properties.

Regarding the 10% higher average current density in Pt@rGO with respect to Pt@Graphitene cathode, differences are explained by several factors: (i) a higher Pt@rGO surface area (12.39 m^2/g *vs.* 10.76 m^2/g) as the powder-like material has a larger specific surface area than crystals, (ii) a higher electroactive area of Pt@rGO (1.14 *vs.* 0.69 cm^2), (iii) the Pt in Pt@rGO is less prone to be detached (Fig. 3), and (iv) Pt@rGO crystals are more fragmented, so, the ink and, subsequently, Pt, are more homogeneously distributed (Fig. 4).

The cells with cathodes coated with commercial ink showed an intermediate performance (0.34 mA/cm^2). Previous

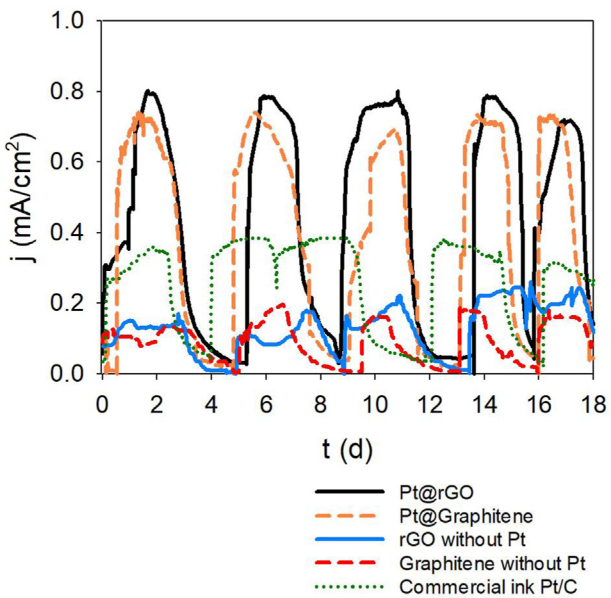

Fig. 7 – Evolution of the current intensity during the last 18 days of stable operation for the different MEC tested with rGO, Graphitene, Pt@rGO and Pt@Graphitene, and standard cathode with commercial ink.

results with the same cells and the commercial ink reached intensities lower than 0.50 mA/cm^2 [62]. The commercial ink contains 10% Pt/90% C and the amount of commercial ink added was calculated so that the commercial and the manufactured materials had the same amount of Pt. Thus, both Pt@rGO and Pt@Graphitene cells reached, for instance, intensities twice higher than these in other works (ranging from 0.03 to 0.64 mA/cm^2) [63,64].

Furthermore, Fig. 7 shows as rGO and Graphitene without Pt also produced current density meaning that these materials can catalyse the reaction in spite of having worse behavior than the functionalized graphenes since Pt is one of the best and most widely used H_2 catalyst.

Table 3 compares current densities found in the literature for H_2 production in similar cells but using different cathodic materials. These results clearly show that the metal-coated cathodes perform better [62–64] than sole carbon-based cathodes [66]. The materials tested in this work were Pt-coated and carbon-based, which increased the cathode performance. Remarkably, Pt@rGO provided the highest values reported (0.78 mA/cm^2) and Pt@Graphitene also reached a high value (0.71 mA/cm^2), similar to the peak value reported for Ni–P coated Ni-foam (0.73 mA/cm^2) [69].

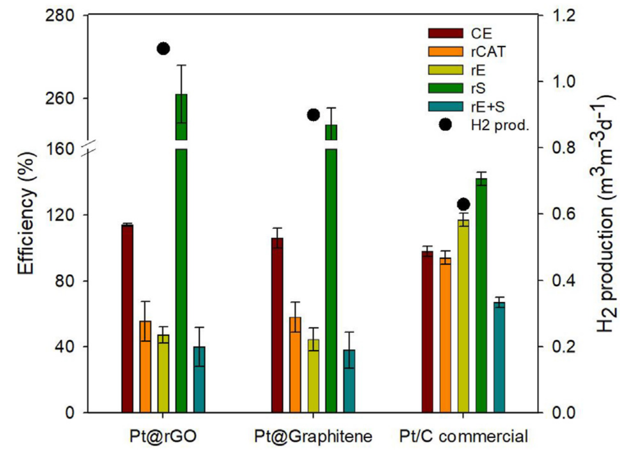

Fig. 8 – The experimental value of CE, r_{CAT}, r_E, r_S, r_{E+S}, and H_2 production of Pt@rGO and Pt@Graphitene. Error bar is the standard deviation for n = 3 measurements.

Fig. 8 shows the conventional MEC performance parameters for the cells with the Pt-functionalized cathode. Both cells resulted in an unexpected excessive CE (more than 100%) and too low r_{CAT} (less than 60%). Unrealistic CE and r_{CAT} results indicate that some of the H_2 generated was scavenged by microorganisms: CE higher than 100% indicates H_2-recycling, whereas r_{CAT} around 50% or less suggests H_2 losses probably because of methanogenesis or homoacetogenesis. This observation is very common in single-chamber cells [8]. In these cases, CE and r_{CAT} are not the most realistic option to evaluate MEC performance.

CE was 114 ± 1% for Pt@rGO and 106 ± 6% for Pt@Graphitene. Hence, the Pt@rGO cell showed a slightly higher H_2-recycling. Such CEs are higher than those reported in previous works [70], which had an average CE between 50 and 74%. For

Table 3 – Comparison of the current density obtained with different cathode materials.

Cathode material	Current density (mA/cm^2)	Ref.
Carbon cloth with Pt@rGO	0.78	This work
Carbon cloth with Pt@Graphitene	0.71	This work
Granular graphite	0.48	[65]
Carbon mesh with activated carbon	<0.1	[66]
Carbon cloth with Pt	0.35	[62]
	0.64	[63]
RuO_2 coated TiO metal	0.35	[64]
Molybdenum disulfide coated stainless steel mesh	0.26	[67]
Nickel foam	0.24	[67]
Stainless steel wool	0.17	[67]
Stainless steel woven mesh	0.48	[68]
Ni–P coated Ni foam	0.73	[69]
Platinum coated stainless steel mesh	0.34	[67]
	0.62	[69]

instance, high CEs have been reported in low-scale lab systems. For example, the CE reached 82% in an 18 mL MEC [71]. On the other hand, a pilot-scale MEC fed with domestic wastewater reached a CE of 41% [72] working with a 100 L MEC or 55% working with a 120 L MEC [73].

Regarding the r_{CAT}, 56 ± 12% and 58 ± 9% were obtained for Pt@rGO and Pt@Graphitene, respectively, indicating potential H_2 consumption. Despite that, the H_2 production rate (HPR) was 1.1 ± 0.2 $m^3\ m^{-3}\ d^{-1}$ and 0.9 ± 0.3 $m^3\ m^{-3}\ d^{-1}$ in the cells with a Pt@rGO-coated cathode and with a Pt@Graphitene-coated cathode, respectively. Since the cell with the Pt/C commercial coating did not have H_2-recycling, only a 28% lower HPR than that of Pt@rGO or Pt@Graphitene was measured. The r_{CAT} in the case of the Pt/C commercial coating was higher because the H_2 losses increase when the HPR is improved. If no H_2 losses were present (i.e. if r_{CAT} was 100%), the HPR obtained for the Pt@rGO-coated cathode would have been around 2.25 $m^3\ m^{-3}\cdot day^{-1}$, which is much higher than that obtained with the commercial ink coating in our previous works with the same configuration [43]. Other works with a similar single-chamber MEC configuration and a carbon cloth cathode treated with a commercial ink to reach 0.5 mg Pt/cm^2 obtained an HPR of 1.99 $m^3\ m^{-3}\cdot day^{-1}$ [74]. Furthermore, other authors obtained these low HPRs using a different substrate [70] like pig slurry (0.079 $m^3\ m^{-3}\cdot day^{-1}$) or anaerobic sludge (0.88 $m^3\ m^{-3}\cdot day^{-1}$). Contrarily, since acetate corresponds to the substrate that generates the highest current density, similar HPRs to those found in our work were found in previous works that used acetate as substrate [75]. With respect to the gas composition, Pt@rGO contained 76 ± 3% of H_2, 17 ± 8% of CO_2, and 7 ± 3% of CH_4 whereas Pt@Graphitene composition was 81 ± 5% of H_2, 16 ± 8% of CO_2, and 3 ± 2% of CH_4. Thus, the relative composition H_2/CH_4 was 0.92 and 0.96 for Pt@rGO and Pt@Graphitene, respectively. Part of the H_2 losses were attributed to methanogenesis.

Conclusions

This work reports the use of two promising nanomaterials, Pt@rGO and Pt@Graphitene, as coating materials for MECs cathodes. Both of them have similar performances regardless of their synthesis procedure.

The Pt-functionalization of these materials was optimized and the percentage of functionalization obtained by ICP-OES (18.4 ± 2.4% for Pt@rGO and 19.7 ± 5.0% for Pt@Graphitene) were higher than metallic functionalization of similar carbonaceous materials. The optical analyses of the different materials showed that Pt@rGO crystals were finer and, thus, easier to disperse and less prone to detach when entering in contact with the mineral medium. TEM images revealed a crystalline structure for both materials and showed that the size of nanoparticles was lower in the case of Pt@rGO (23 ± 5 nm) with respect to that of Pt@Graphitene (32 ± 11 nm). Pt@rGO also showed better results than Pt@Graphitene in terms of surface area (12.39 m^2/g *vs.* 10.76 m^2/g) and electroactive area (1.14 *vs.* 0.69 cm^2). As consequence, Pt@rGO behavior was slightly better than that of Pt@Graphitene. Besides, the cells with functionalized coatings had higher performance in MECs with respect to non-functionalized cathodes and with cathodes coated with the commonly used commercial ink. Pt@rGO and Pt@Graphitene had an average current density of 0.78 and 0.71 mA/cm^2 *vs.* 0.25 and 0.22 mA/cm^2 for rGO and Graphitene because of the higher proportion of metallic Pt (50%) and lower internal resistances of Pt-functionalized cathodes.

Pt@rGO and Pt@Graphitene provided a higher conductivity and a higher active area, thus, a better performance than conventional inks used in coated cathodes. These functionalized conductive materials open new opportunities for on-demand modification of more efficient catalysts, being able to modify both the ink composition and the catalyst itself.

Declaration of competing interest

The authors declare that they have no known competing financial interests or personal relationships that could have appeared to influence the work reported in this paper.

Acknowledgments

This work has been supported by the Spanish Ministry of Economy and Competitiveness (CTQ2017-82404-R) with funds from the European Regional Development Fund. Pilar Sánchez Peña is grateful for the predoctoral grant FI (2018FI_B01161) from the Generalitat de Catalunya. All authors are members of the GENOCOV research group (Grup de Recerca Consolidat de la Generalitat de Catalunya, 2017 SGR 1175, www.genocov.com). We acknowledge the collaboration of Pedro Gómez-Romero, Raul Benages and Carlos Marchante (who provided the graphitene for this study) and GraphCAT project (001-P-001702), cofunded by the ERDF allocated to the ERDF Operational Program of Catalonia 2014-2020, with the support of the Generalitat de Catalunya.

Appendix A. Supplementary data

Supplementary data to this article can be found online at https://doi.org/10.1016/j.ijhydene.2022.03.078.

REFERENCES

[1] Sewsynker Y, Kana EBG, Lateef A. Modelling of biohydrogen generation in microbial electrolysis cells (MECs) using a committee of artificial neural networks (ANNs). Biotechnol Biotechnol Equip 2015;29:1208–15. https://doi.org/10.1080/13102818.2015.1062732.

[2] Haryanto A, Fernando S, Murali N, Adhikari S. Current status of hydrogen production techniques by steam reforming of ethanol: a review. Energy Fuel 2005;19:2098–106. https://doi.org/10.1021/ef0500538.

[3] Lee H-S, Vermaas WFJ, Rittmann BE. Biological hydrogen production: prospects and challenges. Trends Biotechnol 2010;28:262–71. https://doi.org/10.1016/j.tibtech.2010.01.007.

[4] Logan BE, Call D, Cheng S, Hamelers HVM, Sleutels THJA, Jeremiasse AW, et al. Microbial electrolysis cells for high

yield hydrogen gas production from organic matter. Environ Sci Technol 2008;42:8630–40. https://doi.org/10.1021/es801553z.

[5] Gao Y, Ryu H, Santo Domingo JW, Lee H-S. Syntrophic interactions between H2-scavenging and anode-respiring bacteria can improve current density in microbial electrochemical cells. Bioresour Technol 2014;153:245–53. https://doi.org/10.1016/j.biortech.2013.11.077.

[6] Torres CI, Marcus AK, Lee H-S, Parameswaran P, Krajmalnik-Brown R, Rittmann BE. A kinetic perspective on extracellular electron transfer by anode-respiring bacteria. FEMS Microbiol Rev 2010;34:3–17. https://doi.org/10.1111/j.1574-6976.2009.00191.x.

[7] Sánchez-Peña P, Rodriguez J, Montes R, Baeza JA, Gabriel D, Baeza M, et al. Less is more: a comprehensive study on the effects of the number of gas diffusion layers on air–cathode microbial fuel cells. Chemelectrochem 2021;8:3416–26. https://doi.org/10.1002/celc.202100908.

[8] Ruiz Y, Baeza JA, Guisasola A. Revealing the proliferation of hydrogen scavengers in a single-chamber microbial electrolysis cell using electron balances. Int J Hydrogen Energy 2013;38:15917–27. https://doi.org/10.1016/j.ijhydene.2013.10.034.

[9] Lee H-S, Torres CI, Parameswaran P, Rittmann BE. Fate of H2 in an upflow single-chamber microbial electrolysis cell using a metal-catalyst-free cathode. Environ Sci Technol 2009;43:7971–6. https://doi.org/10.1021/es900204j.

[10] Lee H-S, Rittmann BE. Significance of biological hydrogen oxidation in a continuous single-chamber microbial electrolysis cell. Environ Sci Technol 2010;44:948–54. https://doi.org/10.1021/es9025358.

[11] Parameswaran P, Torres CI, Lee H-S, Rittmann BE, Krajmalnik-Brown R. Hydrogen consumption in microbial electrochemical systems (MXCs): the role of homo-acetogenic bacteria. Bioresour Technol 2011;102:263–71. https://doi.org/10.1016/j.biortech.2010.03.133.

[12] Rago L, Ruiz Y, Baeza JA, Guisasola A, Cortés P. Microbial community analysis in a long-term membrane-less microbial electrolysis cell with hydrogen and methane production. Bioelectrochemistry 2015;106. https://doi.org/10.1016/j.bioelechem.2015.06.003.

[13] Yang E, Omar Mohamed H, Park S-G, Obaid M, Al-Qaradawi SY, Castaño P, et al. A review on self-sustainable microbial electrolysis cells for electro-biohydrogen production via coupling with carbon-neutral renewable energy technologies. Bioresour Technol 2021;320:124363. https://doi.org/10.1016/j.biortech.2020.124363.

[14] Dange P, Pandit S, Jadhav D, Shanmugam P, Gupta PK, Kumar S, et al. Recent developments in microbial electrolysis cell-based biohydrogen production utilizing wastewater as a feedstock. Sustainability 2021;13:8796. https://doi.org/10.3390/su13168796.

[15] Rousseau R, Ketep SF, Etcheverry L, Délia M-L, Bergel A. Microbial electrolysis cell (MEC): a step ahead towards hydrogen-evolving cathode operated at high current density. Bioresour Technol Rep 2020;9:100399. https://doi.org/10.1016/j.biteb.2020.100399.

[16] Guo K, Prévoteau A, Rabaey K. A novel tubular microbial electrolysis cell for high rate hydrogen production. J Power Sources 2017;356:484–90. https://doi.org/10.1016/j.jpowsour.2017.03.029.

[17] Guisasola A, Baeza JA, Marone A, Trably É, Bernet N. Opportunities for hydrogen production from urban/industrial wastewater in bioelectrochemical systems. Microb. Electrochem. Technol. Boca Raton: CRC Press; 2020. p. 225–43. https://doi.org/10.1201/9780429487118-15.

[18] Chae K-J, Choi M-J, Kim K-Y, Ajayi FF, Chang I-S, Kim IS. A solar-powered microbial electrolysis cell with a platinum catalyst-free cathode to produce hydrogen. Environ Sci Technol 2009;43:9525–30. https://doi.org/10.1021/es9022317.

[19] Selembo PA, Merrill MD, Logan BE. Hydrogen production with nickel powder cathode catalysts in microbial electrolysis cells. Int J Hydrogen Energy 2010;35:428–37. https://doi.org/10.1016/j.ijhydene.2009.11.014.

[20] Farhangi S, Ebrahimi S, Niasar MS. Commercial materials as cathode for hydrogen production in microbial electrolysis cell. Biotechnol Lett 2014;36:1987–92. https://doi.org/10.1007/s10529-014-1565-7.

[21] Selembo PA, Merrill MD, Logan BE. The use of stainless steel and nickel alloys as low-cost cathodes in microbial electrolysis cells. J Power Sources 2009;190:271–8. https://doi.org/10.1016/j.jpowsour.2008.12.144.

[22] Xin L, Yang F, Rasouli S, Qiu Y, Li ZF, Uzunoglu A, et al. Understanding Pt nanoparticle anchoring on graphene supports through surface functionalization. ACS Catal 2016;6:2642–53. https://doi.org/10.1021/acscatal.5b02722.

[23] Zhao S, Li Y, Yin H, Liu Z, Luan E, Zhao F, et al. Energy Resources: three-dimensional graphene/Pt nanoparticle composites as freestanding anode for enhancing performance of microbial fuel cells. Sci Adv 2015;1:e1500372. https://doi.org/10.1126/sciadv.1500372.

[24] Li X, Liu X, Wang W, Li L, Lu X. High loading Pt nanoparticles on functionalization of carbon nanotubes for fabricating nonenzyme hydrogen peroxide sensor. Biosens Bioelectron 2014;59:221–6. https://doi.org/10.1016/j.bios.2014.03.046.

[25] Novoselov KS, Jiang D, Schedin F, Booth TJ, Khotkevich VV, Morozov SV, et al. Two-dimensional atomic crystals. Proc Natl Acad Sci Unit States Am 2005;102:10451–3. https://doi.org/10.1073/pnas.0502848102.

[26] Novoselov KS, Geim AK, Morozov SV, Jiang D, Zhang Y, Dubonos SV, et al. Electric field effect in atomically thin carbon films. Science 2004;306:666–9. https://doi.org/10.1126/science.1102896.

[27] Rowley-Neale SJ, Randviir EP, Abo Dena AS, Banks CE. An overview of recent applications of reduced graphene oxide as a basis of electroanalytical sensing platforms. Appl Mater Today 2018;10:218–26. https://doi.org/10.1016/j.apmt.2017.11.010.

[28] Yu W, Sisi L, Haiyan Y, Jie L. Progress in the functional modification of graphene/graphene oxide: a review. RSC Adv 2020;10:15328–45. https://doi.org/10.1039/d0ra01068e.

[29] Ioniță M, Vlăsceanu GM, Watzlawek AA, Voicu SI, Burns JS, Iovu H. Graphene and functionalized graphene: extraordinary prospects for nanobiocomposite materials. Compos B Eng 2017;121:34–57. https://doi.org/10.1016/j.compositesb.2017.03.031.

[30] Li M, Zhou S, Xu M. Graphene oxide supported magnesium oxide as an efficient cathode catalyst for power generation and wastewater treatment in single chamber microbial fuel cells. Chem Eng J 2017;328:106–16. https://doi.org/10.1016/j.cej.2017.07.031.

[31] Yaqoob AA, Ibrahim MNM, Yaakop AS, Umar K, Ahmad A. Modified graphene oxide anode: a bioinspired waste material for bioremediation of Pb2+ with energy generation through microbial fuel cells. Chem Eng J 2021;417:128052. https://doi.org/10.1016/j.cej.2020.128052.

[32] Xin S, Shen J, Liu G, Chen Q, Xiao Z, Zhang G, et al. Electricity generation and microbial community of single-chamber microbial fuel cells in response to Cu2O nanoparticles/reduced graphene oxide as cathode catalyst. Chem Eng J 2020;380:122446. https://doi.org/10.1016/j.cej.2019.122446.

[33] Georgakilas V, Otyepka M, Bourlinos AB, Chandra V, Kim N, Kemp KC, et al. Functionalization of graphene: covalent and non-covalent approaches, derivatives and applications. Chem Rev 2012;112:6156–214. https://doi.org/10.1021/cr3000412.

[34] Xu M, Liang T, Shi M, Chen H. Graphene-like two-dimensional materials. Chem Rev 2013;113:3766–98. https://doi.org/10.1021/cr300263a.
[35] Hou Y, Lv S, Liu L, Liu X. High-quality preparation of graphene oxide via the Hummers' method: understanding the roles of the intercalator, oxidant, and graphite particle size. Ceram Int 2020;46:2392–402. https://doi.org/10.1016/j.ceramint.2019.09.231.
[36] Muñoz J, Brennan LJ, Céspedes F, Gun'ko YK, Baeza M. Characterization protocol to improve the electroanalytical response of graphene-polymer nanocomposite sensors. Compos Sci Technol 2016;125:71–9. https://doi.org/10.1016/j.compscitech.2016.01.018.
[37] Montpart N, Rago L, Baeza JA, Guisasola A. Hydrogen production in single chamber microbial electrolysis cells with different complex substrates. Water Res 2015;68:601–15. https://doi.org/10.1016/j.watres.2014.10.026.
[38] Paredes JI, Villar-Rodil S, Martínez-Alonso A, Tascón JMD. Graphene oxide dispersions in organic solvents. Langmuir 2008;24:10560–4. https://doi.org/10.1021/la801744a.
[39] Liu R, Hu J, Zhu S, Lu J, Zhu H. Synergistically enhanced optical limiting property of graphene oxide hybrid materials functionalized with Pt complexes. ACS Appl Mater Interfaces 2017;9:33029–40. https://doi.org/10.1021/acsami.7b10585.
[40] Baeza JA, Martínez-Miró À, Guerrero J, Ruiz Y, Guisasola A. Bioelectrochemical hydrogen production from urban wastewater on a pilot scale. J Power Sources 2017;356:500–9. https://doi.org/10.1016/j.jpowsour.2017.02.087.
[41] Borole AP, Aaron D, Hamilton CY, Tsouris C. Understanding long-term changes in microbial fuel cell performance using electrochemical impedance spectroscopy. Environ Sci Technol 2010;44:2740–5. https://doi.org/10.1021/es9032937.
[42] Rodríguez J, Mais L, Campana R, Piroddi L, Mascia M, Gurauskis J, et al. Comprehensive characterization of a cost-effective microbial fuel cell with Pt-free catalyst cathode and slip-casted ceramic membrane. Int J Hydrogen Energy 2021. https://doi.org/10.1016/j.ijhydene.2021.01.066.
[43] He Z, Mansfeld F. Exploring the use of electrochemical impedance spectroscopy (EIS) in microbial fuel cell studies. Energy Environ Sci 2009;2:215–9. https://doi.org/10.1039/B814914C.
[44] Manohar AK, Bretschger O, Nealson KH, Mansfeld F. The polarization behavior of the anode in a microbial fuel cell. Electrochim Acta 2008;53:3508–13. https://doi.org/10.1016/j.electacta.2007.12.002.
[45] Muñoz J, Montes R, Baeza M. Trends in electrochemical impedance spectroscopy involving nanocomposite transducers: characterization, architecture surface and bio-sensing. TrAC Trends Anal Chem 2017;97:201–15. https://doi.org/10.1016/j.trac.2017.08.012.
[46] Zhu P, Zhao Y. Cyclic voltammetry measurements of electroactive surface area of porous nickel: peak current and peak charge methods and diffusion layer effect. Mater Chem Phys 2019;233:60–7. https://doi.org/10.1016/j.matchemphys.2019.05.034.
[47] Ambler JR, Logan BE. Evaluation of stainless steel cathodes and a bicarbonate buffer for hydrogen production in microbial electrolysis cells using a new method for measuring gas production. Int J Hydrogen Energy 2011;36:160–6. https://doi.org/10.1016/j.ijhydene.2010.09.044.
[48] Middaugh J, Cheng S, Liu W, Wagner R. How to make cathodes with a diffusion layer for single-chamber microbial fuel cells. 2008.
[49] Mirzaei A, Bang JH, Choi MS, Han S, Lee HY, Kim SS, et al. Changes in characteristics of Pt-functionalized RGO nanocomposites by electron beam irradiation for room temperature NO2 sensing. Ceram Int 2020;46:21638–46. https://doi.org/10.1016/j.ceramint.2020.05.271.
[50] Kuila T, Bose S, Mishra AK, Khanra P, Kim NH, Lee JH. Chemical functionalization of graphene and its applications. Prog Mater Sci 2012;57:1061–105. https://doi.org/10.1016/j.pmatsci.2012.03.002.
[51] Chen Y, Xie B, Ren Y, Yu M, Qu Y, Xie T, et al. Designed nitrogen doping of few-layer graphene functionalized by selective oxygenic groups. Nanoscale Res Lett 2014;9:646. https://doi.org/10.1186/1556-276X-9-646.
[52] Wen Q, Wang S, Yan J, Cong L, Chen Y, Xi H. Porous nitrogen-doped carbon nanosheet on graphene as metal-free catalyst for oxygen reduction reaction in air-cathode microbial fuel cells. Bioelectrochemistry 2014;95:23–8. https://doi.org/10.1016/j.bioelechem.2013.10.007.
[53] Leela A, Reddy M, Srivastava A, Gowda SR, Gullapalli H, Dubey M, et al. Synthesis of nitrogen-doped graphene films For Lithium Battery Application. ACS Nano 2020;4:18. https://doi.org/10.1021/nn101926g.
[54] Wei D, Liu Y, Wang Y, Zhang H, Huang L, Yu G. Synthesis of N-doped graphene by chemical vapor deposition and its electrical properties. Nano Lett 2009;9:1752–8. https://doi.org/10.1021/nl803279t.
[55] Zhu M, Li Z, Xiao B, Lu Y, Du Y, Yang P, et al. Surfactant assistance in improvement of photocatalytic hydrogen production with the porphyrin noncovalently functionalized graphene nanocomposite. ACS Appl Mater Interfaces 2013;5:1732–40. https://doi.org/10.1021/am302912v.
[56] Ramanathan T, Abdala AA, Stankovich S, Dikin DA, Herrera-Alonso M, Piner RD, et al. Functionalized graphene sheets for polymer nanocomposites. Nat Nanotechnol 2008;3:327–31. https://doi.org/10.1038/nnano.2008.96.
[57] Kocha SS, Zack JW, Alia SM, Neyerlin KC, Pivovar BS. Influence of ink composition on the electrochemical properties of Pt/C electrocatalysts. ECS Trans 2013;50:1475–85. https://doi.org/10.1149/05002.1475ecst.
[58] Sealy C. The problem with platinum. Mater Today 2008;11:65–8. https://doi.org/10.1016/S1369-7021(08)70254-2.
[59] Liu W, Ma Y, Sun G, Wang S, Deng J, Wei H. Molecularly imprinted polymers on graphene oxide surface for EIS sensing of testosterone. Biosens Bioelectron 2017;92:305–12. https://doi.org/10.1016/j.bios.2016.11.007.
[60] Bonanni A, Loo AH, Pumera M. Graphene for impedimetric biosensing. TrAC Trends Anal Chem (Reference Ed) 2012;37:12–21. https://doi.org/10.1016/j.trac.2012.02.011.
[61] Kretzschmar J, Harnisch F. Electrochemical Impedance Spectroscopy on biofilm electrodes – conclusive or euphonious? Curr Opin Electrochem 2021:100757. https://doi.org/10.1016/j.coelec.2021.100757.
[62] Ruiz Y, Baeza JA, Guisasola A. Microbial electrolysis cell performance using non-buffered and low conductivity wastewaters. Chem Eng J 2016;289:341–8. https://doi.org/10.1016/j.cej.2015.12.098.
[63] Kiely PD, Cusick RD, Call DF, Selembo PA, Regan JM, Logan BE. Anode microbial communities produced by changing from microbial fuel cell to microbial electrolysis cell operation using two different wastewaters. Bioresour Technol 2011;102:388–94. https://doi.org/10.1016/j.biortech.2010.05.019.
[64] Pasupuleti SB, Srikanth S, Venkata Mohan S, Pant D. Development of exoelectrogenic bioanode and study on feasibility of hydrogen production using abiotic VITO-CoRE™ and VITO-CASE™ electrodes in a single chamber microbial electrolysis cell (MEC) at low current densities. Bioresour Technol 2015;195:131–8. https://doi.org/10.1016/j.biortech.2015.06.145.
[65] Cerrillo M, Viñas M, Bonmatí A. Anaerobic digestion and electromethanogenic microbial electrolysis cell integrated system: increased stability and recovery of ammonia and

methane. Renew Energy 2018;120:178–89. https://doi.org/10.1016/j.renene.2017.12.062.
[66] Luo S, Liu F, Fu B, He K, Yang H, Zhang X, et al. Onset investigation on dynamic change of biohythane generation and microbial structure in dual-chamber versus single-chamber microbial electrolysis cells. Water Res 2021;201:117326. https://doi.org/10.1016/j.watres.2021.117326.
[67] Ribot-Llobet E, Nam J-Y, Tokash JC, Guisasola A, Logan BE. Assessment of four different cathode materials at different initial pHs using unbuffered catholytes in microbial electrolysis cells. Int J Hydrogen Energy 2013;38:2951–6. https://doi.org/10.1016/j.ijhydene.2012.12.037.
[68] Zhou R, Zhou S, He C. Quantitative evaluation of effects of different cathode materials on performance in Cd(II)-reduced microbial electrolysis cells. Bioresour Technol 2020;307:123198. https://doi.org/10.1016/j.biortech.2020.123198.
[69] Li F, Liu W, Sun Y, Ding W, Cheng S. Enhancing hydrogen production with Ni–P coated nickel foam as cathode catalyst in single chamber microbial electrolysis cells. Int J Hydrogen Energy 2017;42:3641–6. https://doi.org/10.1016/j.ijhydene.2016.10.163.
[70] Hua T, Li S, Li F, Zhou Q, Ondon BS. Microbial electrolysis cell as an emerging versatile technology: a review on its potential application, advance and challenge. J Chem Technol Biotechnol 2019;94:1697–711. https://doi.org/10.1002/jctb.5898.
[71] Call DF, Wagner RC, Logan BE. Hydrogen production by geobacter species and a mixed consortium in a microbial electrolysis cell. Appl Environ Microbiol 2009;75:7579–87. https://doi.org/10.1128/AEM.01760-09.
[72] Heidrich ES, Edwards SR, Dolfing J, Cotterill SE, Curtis TP. Performance of a pilot scale microbial electrolysis cell fed on domestic wastewater at ambient temperatures for a 12 month period. Bioresour Technol 2014;173:87–95. https://doi.org/10.1016/j.biortech.2014.09.083.
[73] Heidrich ES, Dolfing J, Scott K, Edwards SR, Jones C, Curtis TP. Production of hydrogen from domestic wastewater in a pilot-scale microbial electrolysis cell. Appl Microbiol Biotechnol 2013;97:6979–89. https://doi.org/10.1007/s00253-012-4456-7.
[74] Call D, Logan BE. Hydrogen production in a single chamber microbial electrolysis cell lacking a membrane. Environ Sci Technol 2008;42:3401–6. https://doi.org/10.1021/es8001822.
[75] Kadier A, Kalil MS, Abdeshahian P, Chandrasekhar K, Mohamed A, Azman NF, et al. Recent advances and emerging challenges in microbial electrolysis cells (MECs) for microbial production of hydrogen and value-added chemicals. Renew Sustain Energy Rev 2016;61:501–25. https://doi.org/10.1016/j.rser.2016.04.017.